HHS Public Access

Author manuscript

J Nucl Med. Author manuscript; available in PMC 2017 May 30.

Published in final edited form as:

J Nucl Med. 2015 June ; 56(6): 908–913. doi:10.2967/jnumed.115.155812.

Small-Animal PET Imaging of Pancreatic Cancer Xenografts Using a ^{64}Cu-Labeled Monoclonal Antibody, MAb159

Hui Wang[*,1], **Dan Li**[*,2,3,4], **Shuanglong Liu**[3], **Ren Liu**[5], **Hong Yuan**[1], **Valery Krasnoperov**[6], **Hong Shan**[2,4], **Peter S. Conti**[3], **Parkash S. Gill**[5], and **Zibo Li**[1,3]

[1]Department of Radiology and Biomedical Research Imaging Center, University of North Carolina at Chapel Hill, Chapel Hill, North Carolina

[2]Department of Radiology, Third Affiliated Hospital of Sun Yat-sen University, Guangzhou, China

[3]Molecular Imaging Center, Department of Radiology, University of Southern California, Los Angeles, California

[4]Guangdong Provincial Engineering Research Center of Molecular Imaging, Guangzhou, China

[5]Department of Pathology, University of Southern California, Los Angeles, California

[6]Vasgene Therapeutics Inc., Los Angeles, California

Abstract

Overexpression of the GRP78 receptor on cell surfaces has been linked with tumor growth, metastasis, and resistance to therapy. We developed a ^{64}Cu-labeled probe for PET imaging of tumor GRP78 expression based on a novel anti-GRP78 monoclonal antibody, MAb159.

Methods—MAb159 was conjugated with the ^{64}Cu-chelator DOTA through lysines on the antibody. DOTA–human IgG was also prepared as a control that did not bind to GRP78. The resulting PET probes were evaluated in BXPC3 pancreatic cancer xenografts in athymic nude mice.

Results—The radiotracer was synthesized with a specific activity of 0.8 MBq/μg of antibody. In BXPC3 xenografts, ^{64}Cu-DOTA-MAb159 demonstrated prominent tumor accumulation (4.3 ± 1.2, 15.4 ± 2.6, and 18.3 ± 1.0 percentage injected dose per gram at 1, 17, and 48 after injection, respectively). In contrast, ^{64}Cu-DOTA–human IgG had low BXPC3 tumor accumulation (4.8 ± 0.5, 7.5 ± 0.7, and 4.6 ± 0.8 percentage injected dose per gram at 1, 17, and 48 h after injection, respectively).

Conclusion—We demonstrated that GRP78 can serve as a valid target for pancreatic cancer imaging. The success of this approach will be valuable for evaluating disease course and therapeutic efficacy at the earliest stages of anti-GRP78 treatment. Moreover, these newly

For correspondence or reprints contact either of the following: Zibo Li, Department of Radiology and Biomedical Research Imaging Center, University of North Carolina-Chapel Hill, 125 Mason Farm Rd., Marsico Hall, Ste. 1200, Chapel Hill, NC 27599. ziboli@med.unc.edu; Hong Shan, Department of Radiology, Third Affiliated Hospital of Sun Yat-sen University, Guangzhou, 510630, China. shanhong@mail.sysu.edu.cn.

*Contributed equally to this work.

Disclosure: No other potential conflict of interest relevant to this article was reported.

developed probes may have important applications in other types of cancer overex-pressing GRP78.

Keywords

GRP78; PET; ^{64}Cu; pancreatic cancer

Pancreatic cancer is the fifth leading cause of cancer-related death, because it is resistant to chemotherapy and often is not detected until a late stage, when metastases are present (1,2). Surgical treatment provides the best prognosis for patients who have early-stage disease. Thus, new imaging methods for early detection of pancreatic cancer, and clinically effective methods of monitoring response to therapy, are critical to increasing survival in pancreatic cancer patients.

The glucose-regulated protein GRP78, also known as immuno-globulin heavy-chain binding protein, was discovered in the late 1970s as a cellular protein induced by glucose starvation. In human cancers, an elevated GRP78 level generally correlates with higher pathologic grade, recurrence, and poor survival in patients with breast, liver, prostate, colon, or gastric cancers (3). Although GRP78 expression is maintained at a low basal level in major adult organs such as the brain, lung, and heart, it is strongly induced in tumors (4,5). In addition, glucose starvation resulting from poor perfusion within tumors could induce surface relocalization of GRP78 (3,6,7).

Recently, a monoclonal antibody, MAb159, against GRP78 was developed to target surface GRP78 and block its oncogenic functions (8). MAb159 has been found to suppress phosphatidylinositol-3′-kinase/protein kinase B (Akt) signaling, induce apoptosis, and induce tumor regression in xenografts and spontaneous tumor models. The humanized MAb159 retains its GRP78-binding affinity and efficacy and is nontoxic to normal organs. MAb159 will soon be tested on humans.

A noninvasive PET imaging probe that can visualize and quantify GRP78 expression in vivo is needed to meet the future demand for anti-GRP78 cancer therapy. Herein, we report a novel MAb159-based PET probe and its small-animal imaging results.

Materials and Methods

Unless noted otherwise, all chemicals were of analytic grade and purchased from Sigma-Aldrich. DOTA analogs were purchased from Macrocyclics, Inc. Size-exclusion PD-10 columns were purchased from GE Healthcare. The monoclonal antibody, MAb159, was kindly provided by Vasgene Therapeutics, Inc. Human IgG (hIgG) was purchased from Rockland Immunochemicals Inc. CD31 antibody was from BD Pharmingen. The secondary antibodies goat anti-human Alexa Fluor 568 and goat anti-rat Alexa Fluor 488 were purchased from Invitrogen. Cy5.5 N-hydroxysuccinimide (Cy5.5-NHS) ester was purchased from Lumiprobe Corp. ^{64}Cu was obtained from Washington University and the University of Wisconsin. ^{64}Cu was produced using the ^{64}Ni (p,n) ^{64}Cu nuclear reaction and supplied in high specific activity as $^{64}CuCl_2$ in 0.1N HCl.

Chemistry and Radiochemistry

MAb159 and hIgG were conjugated with DOTA using a method published previously (9). DOTA was first activated to DOTA-*N*-hydroxysulfosuccinimidyl (DOTA-NHS) as previously reported (10). Without purification, DOTA-NHS was cooled to 4°C and added to the MAb159 or hIgG in 0.1 M borate buffer (pH 8.5). The reaction mixture was incubated at 4°C for 10 h. DOTA-MAb159 or DOTA-hIgG conjugates were purified using a PD-10 column and concentrated by a Centricon filter (Millipore). The final concentration was calculated on the basis of ultraviolet absorbance at 280 nm using unconjugated antibody of known concentrations as a standard. Both DOTA-MAb159 and DOTA-hIgG were labeled with ^{64}Cu using the same method. The DOTA-MAb159 or DOTA-hIgG (25–50 μg) was added to $^{64}CuCl_2$ (37–74 MBq of ^{64}Cu). The reaction mixture was adjusted to pH 5.5 with 0.1N sodium acetate and incubated for 1 h at 40°C with constant shaking. The ^{64}Cu-labeled antibody conjugates were then purified by a PD-10 column using 1× phosphate-buffered saline as the eluent. The radioactive fraction containing ^{64}Cu-DOTA-MAb159 or ^{64}Cu-DOTA-hIgG was collected for further in vitro and in vivo experiments. 5(6)-carboxyfluorescein (FAM)-MAb159 was synthesized as reported previously (11,12). FAM succinimidyl ester (FAM-NHS) and MAb159 were mixed at a ratio of 1:1 at pH 8.5. FAM-MAb159 was obtained after incubation at room temperature for 1.5 h and purification with a PD-10 column. Synthesis of Cy5.5-MAb159 and Cy5.5-hIgG is described in supplemental materials (available at http://jnm.snmjournals.org).

Cell Lines and Animal Model

A human pancreatic cancer cell line (BXPC3) and human lung cancer cell line (NCI-H249) were obtained from American Type Culture Collection and cultured under the recommended conditions. Tumor models were established in 4- to 6-wk-old female athymic nude mice obtained from Harlan. Cells were used for in vitro and in vivo experiments when they reached 80%–90% confluence. The GRP78 expression levels on cell lines under high- or low-glucose conditions were evaluated using Western blotting. In brief, approximately 20 μg of whole-cell lysates were run on 4%–20% tris-glycine gradient gel (Bio-Rad) and transferred onto nitrocellulose membrane (Bio-Rad). The membrane was blocked with 5% nonfat dry milk in Tris-buffered saline and 0.05% polysorbate-20 for 40 min and then incubated overnight with a 1 μg/mL concentration of primary antibody at 4°C. The membrane was washed 3 times for 10 min each and incubated with secondary horseradish peroxidase–labeled or IRDye-labeled antibody for 40 min. After 3 washings with Tris-buffered saline and 0.05% polysorbate-20, horseradish peroxidase signal was detected using Femto maximum-sensitivity chemiluminescent sub-strate (Thermo Scientific) and IRDye signal was detected by Odyssey (LICOR).

To generate the BXPC3 tumor model, 4- to 6-wk-old female *nu/nu* mice (Harlan) were each subcutaneously inoculated in the front flank with 2×10^6 BXPC3 cells suspended in 100 μL of phosphate-buffered saline. Tumor size was monitored every other day, and the mice were used for in vivo studies when the tumors reached 4–6 mm in diameter (typically at 3–5 wk after inoculation of the cancer cells). The establishment of other subcutaneous tumor xenografts is described in the supplemental materials.

In Vitro Assays

The binding affinity of DOTA-MAb159 or DOTA-hIgG to GRP78 was evaluated through the bead-based binding assay following a procedure reported in the literature (11,13). The GRP78-binding activity of unmodified MAb159 and hIgG was also evaluated as a positive and negative control, respectively. Cellular uptake was analyzed as previously described (14). BXPC3 tumor cells were cultured in either high-glucose or glucose-free Dulbecco modified Eagle medium supplemented with 10% fetal bovine serum. FAM-MAb159 (10 μg/mL) was added to the BXPC3 cells. After incubation at 37°C for 0.5 h, the cells were fixed with 2% paraformaldehyde and stained with 4′-6-diamidino-2-phenylindole. The cell uptake images were obtained with an Eclipse 80i fluorescence microscope (Nikon).

PET Imaging and Image Analysis

PET imaging and image analysis were performed using an R4 PET rodent scanner (Siemens Medical Solutions) or an eXplore Vista PET/ CT rodent scanner (GE Healthcare) as previously reported (10,15). In brief, 3.7–7.4 MBq of PET probe were intravenously injected into each mouse under isoflurane anesthesia. Static scans were acquired at 1, 17, and 48 h after injection. The images were reconstructed by 2-dimensional ordered-subsets expectation maximum. For each PET scan, regions of interest were drawn over the tumor and major organs on decay-corrected whole-body coronal images. The radioactivity concentration in each organ was obtained from the mean values within the multiple regions of interest and then converted to percentage injected dose per gram of tissue (%ID/g) (16). After all PET scans had been performed, the animals were sacrificed; blood, the heart, and other major organs were collected and weighed wet. The radioactivity in the tissue was measured using a γ counter (Packard Instruments). The results are presented as %ID/g. Values are expressed as mean ± SD for 3 animals.

Immunofluorescence Staining of Tumor Tissues

For the antibody distribution assay in tumor, 30 μg of DOTA-MAb159 or DOTA-hIgG were injected via the tail vein into each BXPC3 tumor– bearing mouse. At 48 h after injection, the mice were sacrificed and the tumors dissected. Frozen sections of tumor (8 μm) were fixed in 4% paraformaldehyde (Electron Microscopy Sciences) and blocked with 10% normal goat serum (Invitrogen). Sections were then incubated with anti-CD31 primary antibody overnight at 4°C, followed by the corresponding secondary antibody for 1 h at room temperature. Subsequently, the slides were covered with Vecta-shield mounting medium (Vector Labs) with 4,6-diamino-2-phenylindole and images were obtained with an Eclipse 80i fluorescence microscope (Nikon). Secondary antibody goat anti-human Alexa Fluor 568 and goat anti-rat Alexa Fluor 488 were used to detect antibodies (hIgG or MAb159) and CD31, respectively. Preparation of HT29 and PC3 tumor sections and CD31 staining of these sections are described in the supplemental materials.

Statistical Analysis

Quantitative data were expressed as mean ± SD. Means were compared using 1-way ANOVA and the Student *t* test. *P* values of less than 0.05 were considered statistically significant.

Results

Chemistry and Radiochemistry

In the DOTA conjugation reaction, 20 equivalents of DOTA-NHS were added to the MAb159 or hIgG under slightly basic conditions (Fig. 1). After a 10-h incubation at 4°C, PD-10 purification afforded DOTA-MAb159 and DOTA-hIgG in 82% and 75% yield, respectively. The average number of DOTAs in each antibody was not determined. ^{64}Cu labeling for DOTA-MAb159 and DOTA-hIgG was achieved in pH 5.5 sodium acetate solution with decay-corrected yields of 56% and 42%, respectively. The specific activity of the final product was estimated to be 0.8 MBq/μg of antibody.

Western Blotting

Measured by Western blotting, GRP78 expression levels were determined in a human pancreatic cancer cell line (BXPC3) and a human lung cancer cell line (NCI-H249) (Fig. 2). The cells were cultured in either high-glucose or glucose-free Dulbecco modified Eagle medium supplemented with 10% fetal bovine serum. The glucose-free conditions were used to mimic a nutrient-deprived tumor microenvironment, which reports have shown recruits a greater amount of MAb159 to the surface of cancer cells under stress (17,18). Both BXPC3 and NCI-H249 cultured in the high-glucose medium showed GRP78 expression (Fig. 2A). As expected, cells cultured in glucose-free medium showed more than 100% GRP78 expression when β-actin was used as an internal standard for quantification (Fig. 2B). With the Western blot results in hand, we chose the BXPC3 cell line for the following in vivo study.

In Vitro Characterization of MAb159 Probes

To prove that labeling of DOTA did not alter the activity of MAb159, we performed a binding affinity experiment with unlabeled MAb159 as a reference. Setting MAb159 as 100%, DOTA-MAb159 retained 85.35% 6 4.10% binding activity ($n = 3$). As a negative control, DOTA-hIgG showed negligible binding to GRP78 (0.055% 6 0.001%, $n = 3$). These results confirmed that DOTA has a minimum effect in reducing the binding affinity of MAb159 to GRP78 receptor. In addition, the cellular uptake of FAM-MAb159 was also tested on BXPC3 tumor cells cultured in both high-glucose and glucose-free medium (Fig. 3). In the high-glucose group, relatively low cell uptake was observed. In contrast, the glucose-free group showed a much higher level of FAM-MAb159 uptake. Considering the differences in expression level of GRP78 between the high-glucose and glucose-free groups, we concluded that FAM-MAb159 uptake is specific to GRP78 receptors.

Small-Animal PET and Image Analysis

The tumor-targeting efficacy of ^{64}Cu-DOTA-MAb159 was evaluated by static small-animal PET scans in BXPC3 tumor– bearing mice. Representative decay-corrected coronal PET images obtained at different time points are shown in Figure 4. ^{64}Cu-DOTA-hIgG was used as a negative control for side-by-side comparison. At 1 h after injection, both ^{64}Cu-DOTA-MAb159 and ^{64}Cu-DOTA-hIgG were circulating mainly in the blood pool. The BXPC3 tumors were clearly visualized in the ^{64}Cu-DOTA-MAb159 group, with good tumor-to-

background contrast at late time points. The activity accumulation of ^{64}Cu-DOTA-MAb159 in BXPC3 tumors was 4.3 ± 1.2, 15.4 ± 2.6, and 18.3 ± 1.0 %ID/g at 1, 17, and 48 h after injection, respectively. In contrast, the activity accumulation of ^{64}Cu-DOTA-hIgG in BXPC3 tumors was 4.8 ± 0.5, 7.5 ± 0.7, and 4.6 ± 0.8 %ID/g at 1, 17, and 48 h after injection, respectively. Except for the 1-h time point, ^{64}Cu-DOTA-MAb159 demonstrated significantly higher tumor uptake than ^{64}Cu-DOTA-hIgG ($P < 0.05$). Other than tumor uptake, both ^{64}Cu-DOTA-MAb159 and ^{64}Cu-DOTA-hIgG showed similar distribution patterns in normal organs such as the liver and kidney and in muscle. At the 1-h time point, tumor-to-muscle contrast for ^{64}Cu-DOTA-MAb159 was 1.40 ± 0.30. With the continued accumulation of ^{64}Cu-DOTA-MAb159 in BXPC3 tumors, the tumor-to-muscle ratio increased to 7.4 ± 4.6 at 17 h after injection and to 11.5 ± 7.2 at 48 h after injection.

To further validate the PET quantification, biodistribution by direct tissue sampling was determined immediately after the PET scans (Fig. 5). BXPC3 tumor uptake for ^{64}Cu-DOTA-MAb159 and ^{64}Cu-DOTA-hIgG was 13.1 ± 1.7 and 5.3 ± 0.6 %ID/g, respectively. In contrast, uptake in other normal organs did not significantly differ between ^{64}Cu-DOTA-MAb159 and ^{64}Cu-DOTA-hIgG ($P > 0.05$). The biodistribution results were consistent with the PET quantification.

The tumor-targeting efficacy of ^{64}Cu-DOTA-MAb159 was also evaluated by static small-animal PET scans of mice bearing human colorectal cancer HT29 and human prostate cancer PC-3 tumors. Representative PET images are shown in Supplemental Figure 1. The activity accumulation of ^{64}Cu-DOTA-MAb159 in PC3 was 2.1 ± 0.5, 3.8 ± 0.5, and 4.2 ± 0.1 %ID/g at 1, 24, and 48 h after injection, respectively, which was significantly higher than in muscle (0.4 ± 0.1, 0.5 ± 0.4, and 0.2 ± 0.1 %ID/g at 1, 24, and 48 h after injection, respectively) (Supplemental Fig. 2A). Similar results were observed for HT29 xenografts. The activity accumulation of ^{64}Cu-DOTA-MAb159 in HT29 tumor was 2.6 ± 0.4, 4.4 ± 1.3, and 4.5 ± 1.3 %ID/g at 1, 24, and 48 h after injection, respectively, which was significantly higher than in muscle (0.4 ± 0.1, 0.4 ± 0.1, and 0.2 ± 0.01 %ID/g at 1, 24, and 48 h after injection, respectively) (Supplemental Fig. 2B).

Immunofluorescence Staining of Tumor Tissue

To further confirm that MAb159 targeted GRP78 on tumor cell surfaces in vivo, we stained the tumor tissue using intravenously injected MAb159 as the primary antibody and goat anti-human antibody conjugated with Alexa Fluor as the secondary antibody. Images were obtained under identical conditions and displayed at the same scale so that the relative brightness observed in the images reflected the difference in relative MAb159 and hIgG concentrations (Fig. 6). For MAb159, a strong red signal was observed in tumor tissue, indicating prominent accumulation of the antibody. The negative control hIgG distributed only minimally in BXPC3 tumors. Similar results were observed for the HT29 and PC3 tumor models (Supplemental Fig. 3). Both the biodistribution studies and the immunofluorescence staining studies confirmed that MAb159 was specifically targeting the GRP78 receptor.

Discussion

Accumulative works have demonstrated that GRP78 protein, a master switch in endoplasmic reticulum stress, plays a pivotal role in cancer cell proliferation, angiogenesis, and chemoresistance (6,19,20). GRP78 localizes mainly in the endoplasmic reticulum, but GRP78 can also relocate to the cell membrane. Cell-surface GRP78 expression has been detected in many different cancers, such as breast, liver, prostate, and pancreatic, and has been associated with the development of drug resistance and cell transformation (17,21–23). These findings, coupled with the observation that peptides targeting GRP78 homed predominantly into tumor tissues but much less into normal organs suggest that cell-surface GRP78 might serve as a novel target for cancer-specific imaging and drug delivery. MAb159 specifically recognizes cell-surface GRP78 and thus can be used to image the tumor for personalized medicine and to determine whether the amount of surface GRP78 in the tumor indicates disease progression or response to therapy. In this study, we developed a MAb159-based noninvasive PET imaging probe to visualize and quantify GRP78 expression in tumor-bearing mice in vivo.

In our approach, the novel ^{64}Cu-labeled MAb159 antibody was synthesized and characterized to demonstrate that imaging GRP78 expression with PET is feasible. ^{64}Cu was attached to MAb159 using a commercially available bifunctional chelator, DOTA. The binding activity assay showed that DOTA-MAb159 preserved 85.35% ± 4.10% of GRP78-binding activity, compared with unmodified MAb159. We used glucose-free conditions to mimic nutrient deprivation in the tumor microenvironment, and we performed Western blotting to analyze GFR78 expression levels in tumor cells. The Western blot results demonstrated significantly higher GRP78 expression in tumor cells cultured in glucose-free medium than in tumor cells cultured in high-glucose medium (Fig. 2). The cell uptake study further confirmed that MAb159 could bind to glucose-starved BXPC3 tumor cells, which had a higher GRP78 expression level, but not to BXPC3 tumor cells cultured in high-glucose medium, which had lower GRP78 expression (Fig. 3).

The in vivo small-animal PET imaging study was performed on mice bearing BXPC3 tumor xenografts (Figs. 4 and 7). ^{64}Cu-DOTA-MAb159 and ^{64}Cu-DOTA-hIgG showed similar distribution patterns in normal organs such as the liver and kidney and in muscle. However, ^{64}Cu-DOTA-MAb159 uptake in BXPC3 tumors increased over time, with maximum tumor uptake being 18.3 ± 1.0 %ID/g at 48 h after injection. Both active uptake (by MAb159-GRP78 interaction) and passive uptake (by the enhanced permeability and retention effect) led to ^{64}Cu-DOTA-MAb159 accumulation in BXPC3 tumors. In contrast, accumulation of ^{64}Cu-DOTA-hIgG in tumors was caused only by passive uptake, with a peak of 7.5 ± 0.7 %ID/g at 24 h after injection. Ex vivo biodistribution studies further validated the PET imaging results. BXPC3 tumor uptake of ^{64}Cu-DOTA-MAb159 and ^{64}Cu-DOTA-hIgG was 14.9 ± 0.7 and 3.3 ± 0.6 %ID/g, respectively. Although nontargeting ^{64}Cu-DOTA-hIgG also accumulated somewhat in BXPC3 tumors, the significant difference in uptake between ^{64}Cu-DOTA-MAb159 and ^{64}Cu-DOTA-hIgG would result from the GRP78 targeting. In addition, ^{64}Cu-DOTA-MAb159 showed significantly higher uptake in both HT29 and PC3 xenografts (Supplemental Fig. 1) than in nontargeted tissue such as muscle, further indicating specific GRP78 targeting of ^{64}Cu-DOTA-MAb159. In this study, we used

a subcutaneous tumor model. Although not orthotopic and not representing appropriate sites for human tumors, these models are easy to establish and have predictable and reproducible tumor growth. In addition, by combining ultrasound and photoacoustic imaging, several independent groups have found and measured hypoxia and poor blood perfusion in subcutaneous tumors (24–26). Therefore, subcutaneous xenograft models should be useful in preliminary evaluations of PET imaging of stress-induced GRP78 upregulation using ^{64}Cu-DOTA-MAb159. Although we observed prominent and specific tumor uptake with ^{64}Cu-DOTA-MAb159, DOTA chelating agents may potentially lose ^{64}Cu from the conjugate in vivo, leading to high uptake in the liver. Other stable chelators, including sarcophagine cage, NOTA, or cross-bridged chelators, will be considered in our follow-up study if the agent is used mainly as a diagnostic probe. Nonetheless, DOTA is able to chelate other therapeutic radiometals (such as ^{177}Lu and ^{90}Y), which may allow us translate the DOTA-based imaging agent to a radiotherapeutic agent by changing the radiometal to a therapeutic isotope. We used the universal chelator DOTA, which can complex a wide variety of both imaging and therapeutic radioisotopes. The same DOTA-MAb159 conjugate can therefore readily be used for both imaging and therapeutic applications without significant alteration of its pharmacokinetic and tumor-targeting efficacy.

It has been reported that endoplasmic reticulum stress is activated and expression of GRP78 is upregulated in both acute (27) and chronic (28) rodent pancreatitis models. Therefore, the use of MAb159-based molecular imaging probes may not be advantageous in the differential diagnosis of pancreatic cancer from pancreatitis. However, this issue may be less significant in the clinical application of MAb159-based GRP78 imaging because GRP78 upregulation is associated more with cancer progression and development of chemoresistance than with early differential diagnosis of pancreatic cancer (29). After initially responding, tumors eventually become resistant to chemotherapy, accounting for the death of most cancer patients. As a main regulator of cell stress, GRP78 can serve as a biomarker in progressive and chemoresistant tumors. In this study, we evaluated the feasibility of using only the MAb159-based PET probe for GRP78 imaging. One potential application of MAb159-based GRP78 imaging probes will be monitoring tumor aggressiveness and chemoresistance during treatment. Our preliminary data showed that after treatment with 50 μM gemcitabine for 24 h, HT29 cells demonstrated increased Cy5.5-MAb159 binding (Supplemental Fig. 4) and significantly increased cell uptake of ^{64}Cu-DOTA-MAb159 (Supplemental Fig. 5). In contrast, HT29 cell binding and uptake of Cy5.5-IgG and ^{64}Cu-DOTA-IgG were unchanged or slightly decreased by gemcitabine treatment. Because the cells were not permeabilized in the experiments, the increased binding of Cy5.5-MAb159 indicates that the cell-surface GRP78 level increased after treatment. Although the in vitro data showed promising results, GRP78 expression level is a master switch in endoplasmic reticulum stress and thus will be regulated by many factors, including blood flow, tumor size, and hypoxia. To confirm the correlation between cell-surface GRP78 and treatment results in vivo, our follow-up study will have a more comprehensive experimental design, including a larger sample size, a variety of tumor models, more treatment regimes, the optimal imaging windows, and the correlation between imaging changes and cell-surface GRP78 expression.

Conclusion

We have developed a receptor-targeted PET probe for detection of GRP78 upregulation in pancreatic tumor xenografts and other tumor models. This study showed that ^{64}Cu-DOTA-MAb159, based on a humanized GRP78-specific monoclonal antibody, displays high target specificity both in vitro and in vivo. The potential correlation between cell-surface GRP78 expression levels and tumor chemoresistance in multiple types of cancer makes ^{64}Cu-DOTA-MAb159 a clinically translatable agent for monitoring progression of tumors and development of chemoresistance.

Supplementary Material

Refer to Web version on PubMed Central for supplementary material.

Acknowledgments

This work was supported by the NIBIB (1R01EB014354-01A1), the NCI (P30-CA016086-35-37), the American Cancer Society (12199ss1-MRSG-12-034-01-CCE), Vasgene Therapeutics Inc. (NIH: CA168158-01 and CA171538-01), the National Natural Science Foundation of China (U1032002, 81071206, 81271621, and 81301266), and the Key Clinical Research Project of the Public Health Ministry of China 2010–2012 (164).

References

1. Hidalgo M. Pancreatic cancer. N Engl J Med. 2010; 362:1605–1617. [PubMed: 20427809]
2. Siegel R, Ma J, Zou Z, et al. Cancer statistics, 2014. CA Cancer J Clin. 2014; 64:9–29. [PubMed: 24399786]
3. Fu Y, Lee AS. Glucose regulated proteins in cancer progression, drug resistance and immunotherapy. Cancer Biol Ther. 2006; 5:741–744. [PubMed: 16861902]
4. Dong D, Dubeau L, Bading J, et al. Spontaneous and controllable activation of suicide gene expression driven by the stress-inducible grp78 promoter resulting in eradication of sizable human tumors. Hum Gene Ther. 2004; 15:553–561. [PubMed: 15212714]
5. Li J, Lee B, Lee AS. Endoplasmic reticulum stress-induced apoptosis: multiple pathways and activation of p53-up-regulated modulator of apoptosis (PUMA) and NOXA by p53. J Biol Chem. 2006; 281:7260–7270. [PubMed: 16407291]
6. Lee AS. GRP78 induction in cancer: therapeutic and prognostic implications. Cancer Res. 2007; 67:3496–3499. [PubMed: 17440054]
7. Park HR, Tomida A, Sato S, et al. Effect on tumor cells of blocking survival response to glucose deprivation. J Natl Cancer Inst. 2004; 96:1300–1310. [PubMed: 15339968]
8. Liu R, Li X, Gao W, et al. Monoclonal antibody against cell surface GRP78 as a novel agent in suppressing PI3K/AKT signaling, tumor growth, and metastasis. Clin Cancer Res. 2013; 19:6802–6811. [PubMed: 24048331]
9. Li ZB, Cai W, Cao Q, et al. ^{64}Cu-labeled tetrameric and octameric RGD peptides for small-animal PET of tumor $\alpha_v\beta_3$ integrin expression. J Nucl Med. 2007; 48:1162–1171. [PubMed: 17574975]
10. Liu S, Li D, Huang CW, et al. Efficient construction of PET/fluorescence probe based on sarcophagine cage: an opportunity to integrate diagnosis with treatment. Mol Imaging Biol. 2012; 14:718–724. [PubMed: 22476968]
11. Li D, Liu S, Liu R, et al. Axl-targeted cancer imaging with humanized antibody h173. Mol Imaging Biol. 2014; 16:511–518. [PubMed: 24424460]
12. Li D, Liu S, Liu R, et al. EphB4-targeted imaging with antibody h131, h131-F(ab9)2 and h131-Fab. Mol Pharm. 2013; 10:4527–4533. [PubMed: 24147882]
13. Li D, Liu S, Liu R, et al. Targeting the EphB4 receptor for cancer diagnosis and therapy monitoring. Mol Pharm. 2013; 10:329–336. [PubMed: 23211050]

14. Liu S, Li D, Guo J, et al. Design, synthesis, and validation of Axl-targeted monoclonal antibody probe for microPET imaging in human lung cancer xenograft. Mol Pharm. 2014; 11:3974–3979. [PubMed: 24978094]
15. Liu S, Li Z, Yap LP, et al. Efficient preparation and biological evaluation of a novel multivalency bifunctional chelator for ^{64}Cu radiopharmaceuticals. Chemistry. 2011; 17:10222–10225. [PubMed: 21815227]
16. Wu Y, Zhang X, Xiong Z, et al. microPET imaging of glioma integrin $\alpha_v\beta_3$ expression using ^{64}Cu-labeled tetrameric RGD peptide. J Nucl Med. 2005; 46:1707–1718. [PubMed: 16204722]
17. Ni M, Zhang Y, Lee AS. Beyond the endoplasmic reticulum: atypical GRP78 in cell viability, signalling and therapeutic targeting. Biochem J. 2011; 434:181–188. [PubMed: 21309747]
18. Zhang Y, Liu R, Ni M, et al. Cell surface relocalization of the endoplasmic reticulum chaperone and unfolded protein response regulator GRP78/BiP. J Biol Chem. 2010; 285:15065–15075. [PubMed: 20208072]
19. Li J, Lee AS. Stress induction of GRP78/BiP and its role in cancer. Curr Mol Med. 2006; 6:45–54. [PubMed: 16472112]
20. Li Z. Glucose regulated protein 78: a critical link between tumor microenvironment and cancer hallmarks. Biochim Biophys Acta. 2012; 1826:13–22. [PubMed: 22426159]
21. Dong D, Stapleton C, Luo B, et al. A critical role for GRP78/BiP in the tumor microenvironment for neovascularization during tumor growth and metastasis. Cancer Res. 2011; 71:2848–2857. [PubMed: 21467168]
22. Virrey JJ, Dong D, Stiles C, et al. Stress chaperone GRP78/BiP confers chemore-sistance to tumor-associated endothelial cells. Mol Cancer Res. 2008; 6:1268–1275. [PubMed: 18708359]
23. Wey S, Luo B, Tseng CC, et al. Inducible knockout of GRP78/BiP in the hematopoietic system suppresses Pten-null leukemogenesis and AKT oncogenic signaling. Blood. 2012; 119:817–825. [PubMed: 21937694]
24. Shao Q, Morgounova E, Jiang C, et al. In vivo photoacoustic lifetime imaging of tumor hypoxia in small animals. J Biomed Opt. 2013; 18:076019. [PubMed: 23877772]
25. Lungu GF, Li ML, Xie X, et al. In vivo imaging and characterization of hypoxia-induced neovascularization and tumor invasion. Int J Oncol. 2007; 30:45–54. [PubMed: 17143511]
26. Gerling M, Zhao Y, Nania S, et al. Real-time assessment of tissue hypoxia in vivo with combined photoacoustics and high-frequency ultrasound. Theranostics. 2014; 4:604–613. [PubMed: 24723982]
27. Zeng Y, Wang X, Zhang W, et al. Hypertriglyceridemia aggravates ER stress and pathogenesis of acute pancreatitis. Hepatogastroenterology. 2012; 59:2318–2326. [PubMed: 22389298]
28. Sah RP, Garg SK, Dixit AK, et al. Endoplasmic reticulum stress is chronically activated in chronic pancreatitis. J Biol Chem. 2014; 289:27551–27561. [PubMed: 25077966]
29. Roller C, Maddalo D. The molecular chaperone GRP78/BiP in the development of chemoresistance: mechanism and possible treatment. Front Pharmacol. 2013; 4:10. [PubMed: 23403503]

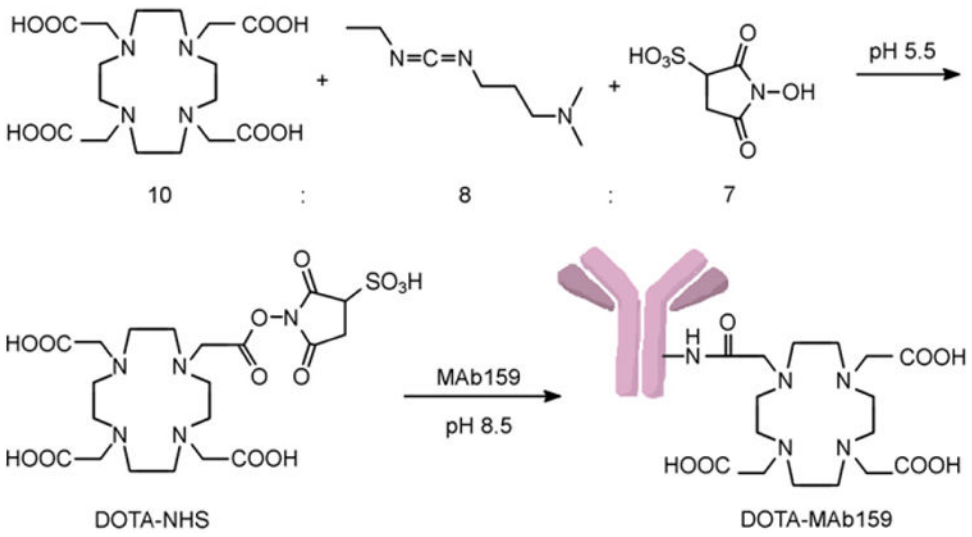

Figure 1.
Conjugation reaction for DOTA-NHS and DOTA-MAb159.

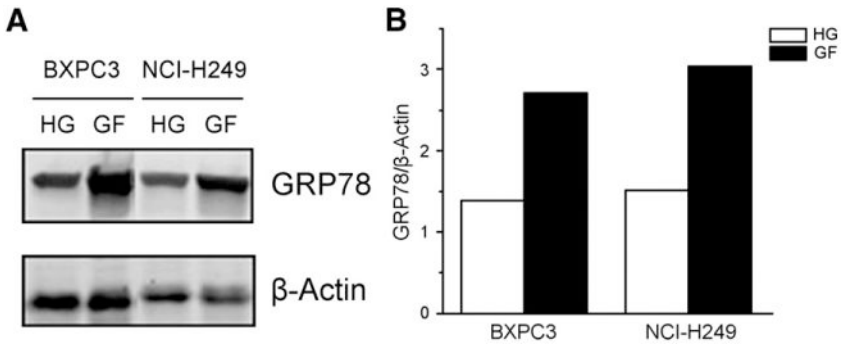

Figure 2.

(A) GRP78 protein levels were determined by Western blotting in BXPC3 and NCI-H249 cell lines. Cells were cultured in either high-glucose (HG) or glucose-free (GF) Dulbecco modified Eagle medium supplemented with 10% fetal bovine serum. (B) GRP78/β-actin ratio quantification of A.

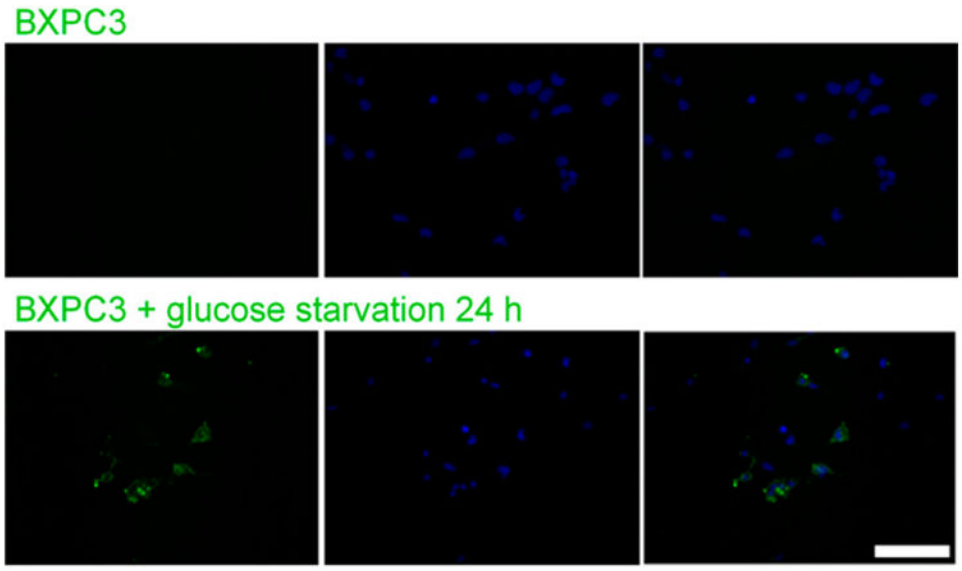

Figure 3.

Cellular uptake analysis of h159-FAM on BXPC3 tumor cells cultured in either high-glucose or glucose-free Dulbecco modified Eagle medium supplemented with 10% fetal bovine serum. Scale bar = 100 μm.

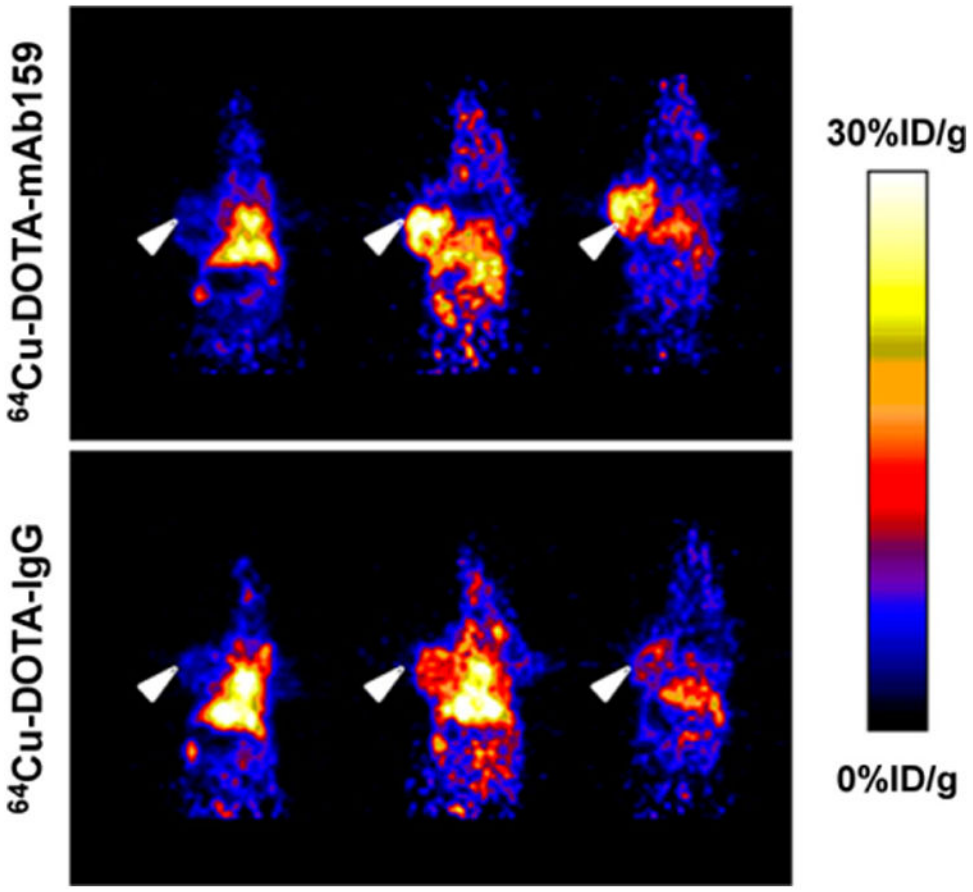

Figure 4.

Decay-corrected whole-body coronal small-animal PET static scans of mice bearing BXPC3 tumors. Images were obtained at 1, 17, and 48 h after injection of ^{64}Cu-DOTA-MAb159 or ^{64}Cu-DOTA-hIgG. Arrowheads indicate tumors.

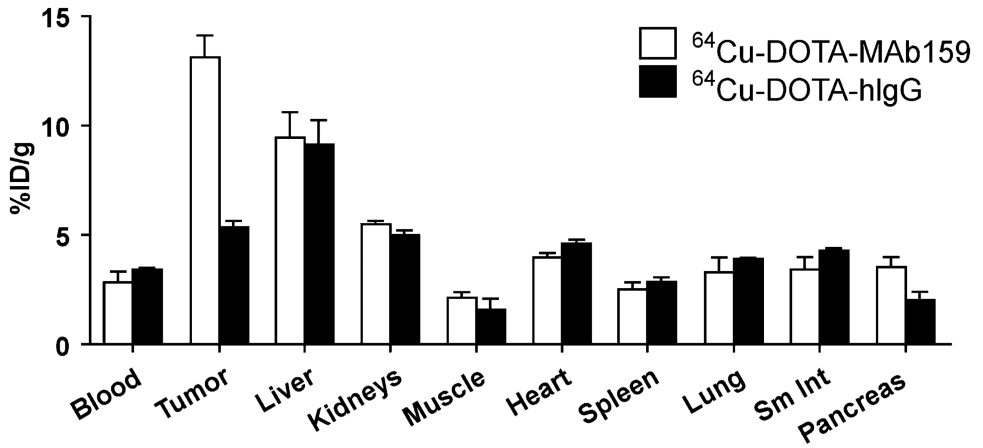

Figure 5.

Direct tissue sampling for radioactivity quantification in major organs of mice bearing BXPC3 tumors at 48 h after injection of ^{64}Cu-DOTA-MAb159 or ^{64}Cu-DOTA-hIgG. Sm Int = small intestine.

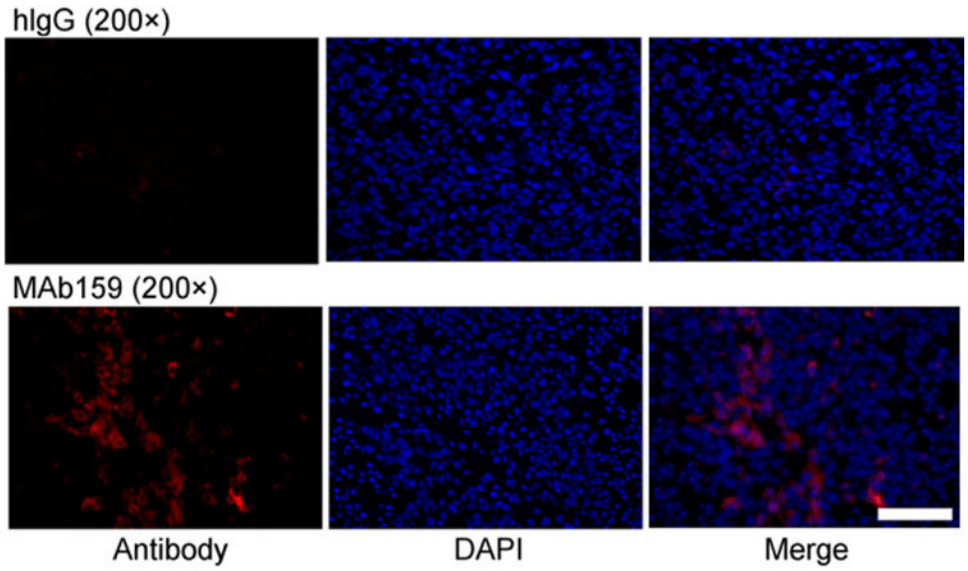

Figure 6.

Antibody distribution analysis on BXPC3 tumor sections 48 h after injection of hIgG or MAb159. Scale bar = 100 μm. DAPI 5 4′-6-diamidino-2-phenylindole.

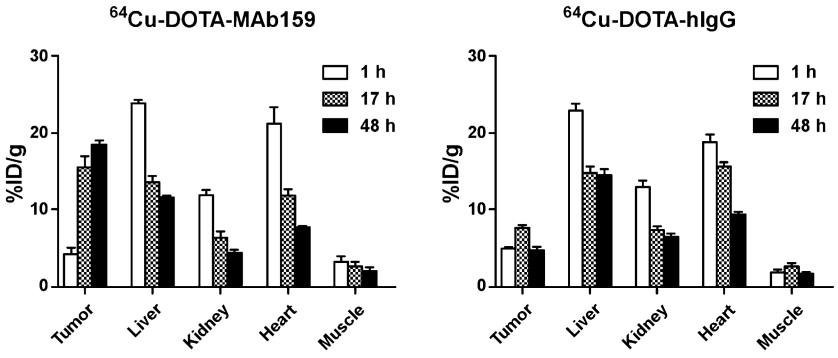

Figure 7.

PET quantification of radioactivity in major organs of mice bearing BXPC3 tumors after injection of ^{64}Cu-DOTA-MAb159 or ^{64}Cu-DOTA-hIgG.